Supplementary Information for: Noise and diffusion of a vibrated self-propelled granular particle

Lee Walsh, Caleb G. Wagner, Sarah Schlossberg, Christopher Olson, Aparna Baskaran, and Narayanan Menon

1 Theoretical model and predictions

Model

An active Brownian particle is parametrized in terms of its position $\vec{r}(t)$ and orientation $\theta(t)$, which evolve according to the following set of stochastic differential equations:

$$\dot{\vec{r}}(t) = v_0\hat{n}(t) + \vec{\eta}(t) \tag{S1}$$

$$\dot{\theta}(t) = \xi(t). \tag{S2}$$

Here v_0 is the magnitude of the self-propulsion velocity, which points in the direction of the unit vector $\hat{n} = \binom{\cos\theta}{\sin\theta}$; and $\vec{\eta}(t)$ and $\xi(t)$ are stochastic terms that indicate Gaussian white noise, with correlations

$$\left\langle \vec{\eta}_\alpha(t)\,\vec{\eta}_\beta(t')\right\rangle = 2D_T\,\delta(t-t')\delta_{\alpha\beta}, \tag{S3}$$

$$\left\langle \xi(t)\,\xi(t')\right\rangle = 2D_R\,\delta(t-t'). \tag{S4}$$

In our case, we modify the above standard description to allow for the temporal correlations in the angular velocity $\xi(t)$. In fact, there is a unique way of doing so, provided we retain the original assumptions that $\xi(t)$ is Markov, Gaussian, and temporally homogeneous (that is, neglecting transient contributions from the initial distribution of $\xi(0)$).[1] Under these assumptions, the correlation is necessarily given as:

$$\left\langle \xi(t)\,\xi(t')\right\rangle = \frac{D_R}{\tau}e^{-|t-t'|/\tau}, \tag{S5}$$

such that τ is the autocorrelation time that we obtain from the experimental data. In summary, equations (S1, S2, S3, and S5) constitute our theoretical model.

Correlation functions

Orientation autocorrelation

We first study the trajectory of a single particle with initial orientation $\theta_0 = \theta(0)$. Because the rotational noise is Gaussian with zero mean, the following identity holds:

$$\langle\cos n\theta(t)\rangle = \cos n\theta_0 \exp\left[-\frac{n^2}{2}\left\langle\Delta\theta(t)^2\right\rangle_c\right], \tag{S6}$$

and likewise for $\langle\sin n\theta(t)\rangle$. Here n may be any integer, and $\left\langle\Delta\theta(t)^2\right\rangle_c$ is the second cumulant of the angular displacement. To obtain this quantity, we integrate the rotational noise:

$$\left\langle\Delta\theta(t)^2\right\rangle_c = \left\langle\Delta\theta(t)^2\right\rangle = \int_0^t\int_0^t \left\langle\xi(s)\,\xi(s')\right\rangle ds\,ds'. \tag{S7}$$

To find the squared angular displacement, we integrate the rotational noise autocorrelation from (S5):

$$\left\langle\Delta\theta(t)^2\right\rangle = \frac{D_R}{\tau}\int_0^t\left[\int_0^{s'} e^{-(s'-s)/\tau}ds + \int_{s'}^t e^{-(s-s')/\tau}ds\right]ds' \tag{S8}$$

$$= 2D_R t - 2D_R\tau\left(1-e^{-t/\tau}\right). \tag{S9}$$

We now return to (S6) with this result, and average over all initial orientations θ_0 to arrive at the correlator:

$$\langle \cos\theta \cos\theta_0 \rangle = \frac{1}{2} \exp\left[-D_R t + D_R \tau \left(1 - e^{-t/\tau} \right) \right], \tag{S10}$$

and likewise for $\langle \sin\theta \sin\theta_0 \rangle$. In terms of $\hat{n}$, we have:

$$\left\langle \hat{n}_\alpha(t)\, \hat{n}_\beta(0) \right\rangle = \frac{\delta_{\alpha\beta}}{2} \exp\left[-D_R t + D_R \tau \left(1 - e^{-t/\tau} \right) \right]. \tag{S11}$$

Displacement–orientation correlation

These results immediately enable us to solve for the displacement–orientation correlation:

$$\langle \vec{r}_\alpha(t) \rangle = \int_0^t v_0 \langle \cos\theta(s) \rangle \, ds + \int_0^t \langle \vec{\eta}(s) \rangle \, ds \tag{S12}$$

$$= \int_0^t v_0 \cos\theta_0 \exp\left[-D_R s + D_R \tau \left(1 - e^{-s/\tau} \right) \right] ds + 0. \tag{S13}$$

Averaging over initial orientations, we obtain

$$\left\langle \vec{r}_\alpha(t)\, \hat{n}_\beta(0) \right\rangle = \delta_{\alpha\beta} \frac{v_0}{2} \int_0^t \exp\left[-D_R s + D_R \tau \left(1 - e^{-s/\tau} \right) \right] ds. \tag{S14}$$

If τ is small, we may throw away the double exponential and evaluate the integral to get

$$\left\langle \vec{r}_\alpha(t)\, \hat{n}_\beta(0) \right\rangle \simeq \frac{v_0}{2D_R} e^{D_R \tau} \left(1 - e^{-D_R t} \right) \delta_{\alpha\beta} \tag{S15}$$

Mean squared displacement

For mean squared displacement, we again integrate to get

$$\left\langle [x(t) - x(0)]^2 \right\rangle = v_0^2 \int_0^t \int_0^t \left\langle \cos\theta(s) \cos\theta(s') \right\rangle ds\, ds' + \int_0^t \int_0^t \left\langle \vec{\eta}(s)\, \vec{\eta}(s') \right\rangle ds\, ds'. \tag{S16}$$

Note that the cross-terms vanish because $\cos\theta(t)$ and $\vec{\eta}(t)$ are independent random variables, and $\langle \vec{\eta}(t) \rangle = 0$. The latter integral is straightforward, giving $2D_T t$. We evaluate the first by the following reasoning from probability theory. Supposing $s > s'$, we write

$$\left\langle \cos\theta(s) \cos\theta(s') \right\rangle = \left\langle \cos\theta(s') \left\langle \cos\theta(s) | \cos\theta(s') \right\rangle \right\rangle \tag{S17}$$

where $\langle \cos\theta(s) | \cos\theta(s') \rangle$ denotes the average of $\cos\theta(s)$ given the (sharp) initial value of $\cos\theta(s')$. This quantity may be evaluated using the results of the previous sections, as follows:

$$\left\langle \cos\theta(s) | \cos\theta(s') \right\rangle = \cos\theta(s') \exp\left[-D_R (s - s') + D_R \tau \left(1 - e^{-(s-s')/\tau} \right) \right]; \tag{S18}$$

$$\left\langle \cos\theta(s) \cos\theta(s') \right\rangle = \left\langle \cos^2\theta(s') \right\rangle \exp\left[-D_R (s - s') + D_R \tau \left(1 - e^{-(s-s')/\tau} \right) \right]; \tag{S19}$$

$$\left\langle \cos^2\theta(s') \right\rangle = \frac{1}{2} + \frac{1}{2} \left\langle \cos 2\theta(s') \right\rangle \tag{S20}$$

$$= \frac{1}{2} + \frac{1}{2} \cos 2\theta_0 \exp\left[-4D_R s' + 4D_R \tau \left(1 - e^{-s'/\tau} \right) \right]. \tag{S21}$$

The analogous expression for $s' > s$ is obtained by swapping s and s'. Now, to render the integral in (S16) tractable, we again take the limit in which τ is very small and drop the superexponential piece. Substituting into (S16) and averaging over θ_0, we obtain

$$\left\langle [x(t) - x(0)]^2 \right\rangle = \left(\frac{v_0}{D_R} \right)^2 e^{\tau D_R} \left(e^{-D_R t} - 1 + D_R t \right) + 2D_T t \tag{S22}$$

We sum over dimensions to obtain the total mean squared displacement:

$$\left\langle [\vec{r}(t)-\vec{r}(0)]^2 \right\rangle = 2\left(\frac{v_0}{D_R}\right)^2 e^{\tau D_R}\left(e^{-D_R t}-1+D_R t\right)+4D_T t. \tag{S23}$$

A new characteristic timescale appears, D_T/v_0^2, which marks the transition from translational diffusion to ballistic motion. Expanding the exponential in (S23) around short time $t \ll 1/D_R$ yields mean squared displacement

$$v_0^2 e^{D_R\tau} t^2 + 4D_T t. \tag{S24}$$

Finally, we consider the longitudinal ($\parallel$) and transverse ($\perp$) components of the mean squared displacement, in the body frame of the particle. To calculate this, we take the expression for $\langle [x(t)-x(0)]^2\rangle$ prior to any averaging over θ_0. The longitudinal component then corresponds to $\theta_0 = 0$, and transverse to $\theta_0 = \pi/2$. This gives

$$\mathrm{msd}_{\perp}^{\parallel} = \ell_p^2 e^{\tau D_R}\left(D_R t - 1 + e^{-D_R t} \pm \frac{1}{12} e^{4\tau D_r}\left(e^{-4D_R t}-4e^{-D_R t}+3\right)\right) + 2D_T t. \tag{S25}$$

The short-time expansion for $t \ll 1/D_R$:

$$\mathrm{msd}_{\perp}^{\parallel} \approx \ell_p^2 e^{D_R\tau}\left(\frac{1}{2}\left(1\pm e^{4\tau D_R}\right)D_R^2 t^2 - \frac{1}{6}\left(1\pm 5e^{4\tau D_R}\right)D_R^3 t^3\right) + 2D_T t \tag{S26}$$

indicates that in the transverse direction, the ballistic regime is suppressed; the ballistic term (quadratic in time) vanishes for uncorrelated white noise ($\tau = 0$), but survives for colored noise ($\tau > 0$).

Since white noise shows cubic behavior in the transverse MSD at short time, it seems at first thought that an obscured cubic regime should indicate the presence of colored noise via a quadratic (ballistic) term. However, for colored noise, the quadratic term has a small negative coefficient, which suppresses MSD at short time such that the MSD grows *faster than cubic* as the cubic term begins to dominate.

2 Experiment and analysis

Experimental configurations

We refer in the paper to six experimental configurations, which give a range of motility parameter values. Each configuration is a different combination of: (i) two variations in the particle design, with different slopes of the beveled nose: particle *a* has slope 69°, *b* has slope 73°; and (ii) three values of peak vibrational acceleration: $\Gamma = 10g$, $15g$, and $20g$.

Data analysis

Image analysis

The position and orientation of a particle in each video frame is resolved in our Python-based tracking software.[2–4] The position $(x,\ y)$ is measured to sub-pixel resolution within the image frame as the intensity-weighted centroid of the segment[5] corresponding to the marked particle. The orientation θ is the arctangent of the mean of the displacement vectors from the center to two corners of the particle.

Velocity

The velocities we report in the analysis are numerical time-derivatives of the measured position and orientation. To calculate the derivative, we convolve position with the derivative of a Gaussian kernel.[6] This gives the velocity effectively averaged over a time $\Delta t = 2\sqrt{3}\sigma$, where σ is the Gaussian's standard deviation. The vibration period $1/f$ sets the relevant physical timescale of our experiment, below which we assume the dynamics are not relevant to our present analysis. Our video frame rate exceeds the vibration time scale, giving a time step of $\delta t = 1/(2.4f)$ between position measurements. Thus, we choose σ such that $\delta t < \Delta t < 1/f$.

Correlations

The correlation functions shown in figures 2(c,d) and 3(a,b,c) of the main text and predicted above in equations (S3, S5, S11, S15, and S23) are calculated from the data as fast-Fourier-transform convolutions[6] of single-particle

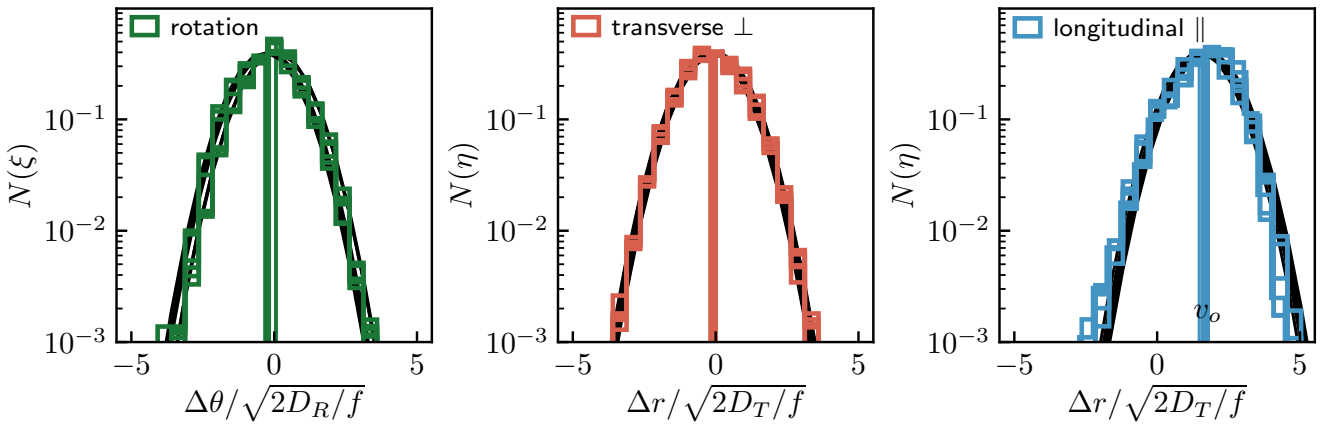

Fig. S1 Histograms for all six experimental configurations. Left panel shows rotational velocity, middle panel shows transverse velocity, and the right panel shows longitudinal velocity. Units are given in terms of the respective coefficients of diffusion.

trajectories.

Fitting

Here we detail the process used to determine the model parameters from fitting the correlation functions (shown in figure 3 of the main text). The three correlation functions (S11, S15, S23) depend, respectively, on one, two, and three parameters. Thus, we introduce one new parameter to each fit in the sequence. In the primary sequence, we fit each function with a single free parameter, fixing any other parameters to their values from the previous fit. In some cases, better fits may be obtained with two free parameters, whose values are generally consistent with those from the single-parameter fits. In figure 3 of the main text, we have plotted single-parameter fits for orientation autocorrelation (S11) and longitudinal displacement (S15), and the two-parameter fit for mean squared displacement (S23). In the parameter comparison (figure 4, main text) we show the parameters from all single-parameter fits and the two-parameter fit to mean squared displacement.

Moments of the noise distributions

config.		rotational (ξ)				self-propulsion (v_0)				transverse ($\eta_\perp$)			
P	Γ	μ	D_R	γ	κ	v_0	σ^2	γ	κ	μ	D_T	γ	κ
a	10	−0.052	0.056	0.122	0.784	0.178	0.003	−0.686	0.361	0.002	0.003	−0.160	0.065
a	15	−0.083	0.065	0.149	0.309	0.186	0.002	−0.571	0.215	0.001	0.005	−0.080	−0.167
a	20	−0.042	0.072	−0.068	1.346	0.192	0.004	−0.496	0.077	−0.008	0.005	0.051	−0.085
b	10	0.013	0.064	−0.094	7.538	0.168	0.001	−0.633	0.395	−0.016	0.004	0.245	0.191
b	15	0.021	0.077	−0.025	6.197	0.170	0.002	−0.268	0.167	−0.018	0.004	0.273	0.155
b	20	0.017	0.096	−0.199	11.477	0.172	0.004	0.016	−0.189	−0.017	0.005	0.194	0.161
		−0.021	0.072	−0.019	4.609	0.178	0.003	−0.439	0.171	−0.009	0.004	0.087	0.053
		±0.040	±0.013	±0.121	±4.124	±0.009	±0.001	±0.244	±0.194	±0.008	±0.001	±0.164	±0.135

Table S1 Moments of the noise distributions: the first four moments (mean μ, variance σ^2, skewness γ, and kurtosis κ) of the three velocity components (rotational ξ, longitudinal $\eta_\parallel$, and transverse $\eta_\perp$) for each of the six experimental configurations, along with the mean and standard deviation over all configurations.

Notwithstanding any correlations, the ABP model assumes noise to come from purely Gaussian distributions with zero mean (excepting longitudinal velocity with mean v_0), zero skewness, and zero excess kurtosis. To clarify the variation and consistency of the distributions, we show supplementary data on all experimental systems. We show the histograms for all configurations overlaid in figure S1, and we report in table S1 the moments of the three velocity distributions for all six experimental configurations. The most substantial and consistent deviation from Gaussian is the skewness of the longitudinal velocity, which shows an excess of velocities below v_0.

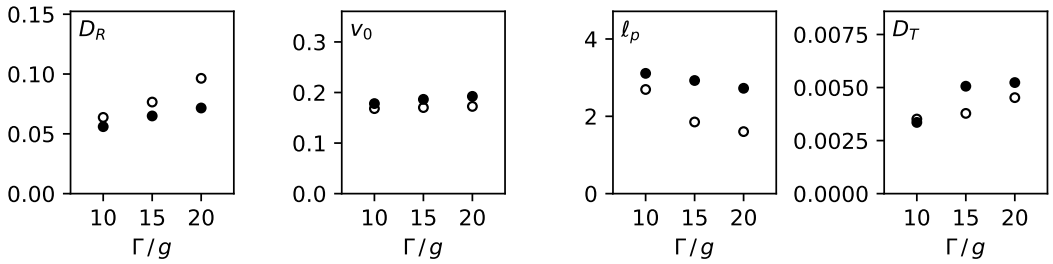

Fig. S2 Self-propulsion parameters as peak vibrational acceleration Γ is varied: the rotational diffusion D_R, self-propulsion velocity v_0, persistence length ℓ_p, and translational diffusion D_T. Note the diffusion coefficients can be tuned somewhat by varying the vibration intensity, but the velocity must be modified by other means (we have used particle geometry).

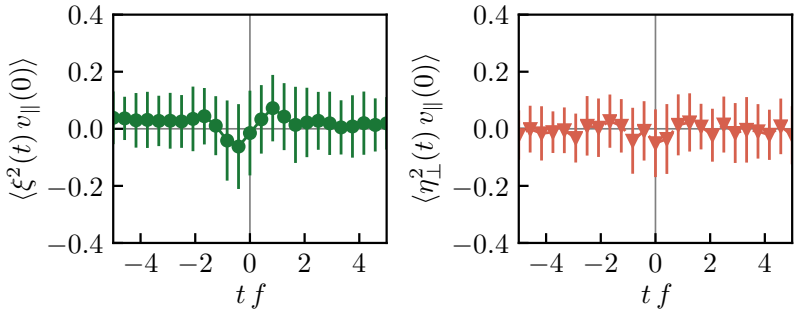

Fig. S3 Velocity–velocity cross-correlations in the noise. Shown are rotational–longitudinal $\langle \xi^2(t)\, v_\parallel(0) \rangle$ and transverse–longitudinal $\langle v_\perp^2(t)\, v_\parallel(0) \rangle$ velocities, normalized by the uncorrelated mean values. Note that the rotational noise shows some correlation with the longitudinal velocity at a timescale $t < \tau$; whereas we observe no systematic cross-correlation between the two components of the translational velocities. Data shown is from the same experimental configuration shown in main text figures 2 and 3.

We resolve the distribution of the net longitudinal velocity ($\dot{\vec{r}}_\parallel$) into two constituent parts: self-propulsion (v_0) and longitudinal diffusion ($\eta_\parallel$), both of which we take to have a distribution of values (whereas the ABP model takes v_0 to be delta-distributed). To calculate these moments, we assume the longitudinal and transverse noise velocities to have equal distributions (i.e., $P(\eta_\parallel) = P(\eta_\perp)$), and thus use the distribution of transverse velocity to remove the contribution of the longitudinal noise from the total longitudinal velocity. This attributes to the distribution of v_0 all of the mean and skewness, and the difference of the variance and kurtosis.

We can tune the values of the moments of these distributions to a limited extent by varying the peak vibrational acceleration Γ. The vibration frequency only rescales the times, so we hold it fixed for the present data. The results of the self-propulsion parameters' dependence on vibration is shown in figure S2. Since this was not the major focus of our study, we only studied three values of Γ for the two particle designs. Nonetheless, some trends are clear: ℓ_p ($= v_0/D_R$), or the persistence length, monotonically increases with Γ. The change in ℓ_p is dominated by change in D_R, while the value of v_0 appears to be unaffected by Γ.

Noise cross-correlations

Skewness and kurtosis in the noise distributions can be interpreted as arising either from a truly non-Gaussian distribution, or from correlations between two sources which add to an effective term, for example $v_\parallel = v_0 + \eta_\parallel$. Therefore, we directly compute the cross-correlations between the noise components: between rotational and longitudinal, and between transverse and longitudinal. One example is shown in figure S3. We find that the cross-correlations are short-lived with a timescale less than τ; and small in magnitude, less than 10% of the auto-correlations in each component.

Spatial inter-particle correlations

As described in the main text, despite the highly correlated nature of the noise source over space as well as time, experimental data clearly demonstrate that such correlations in the driving force do not generate significant spa-

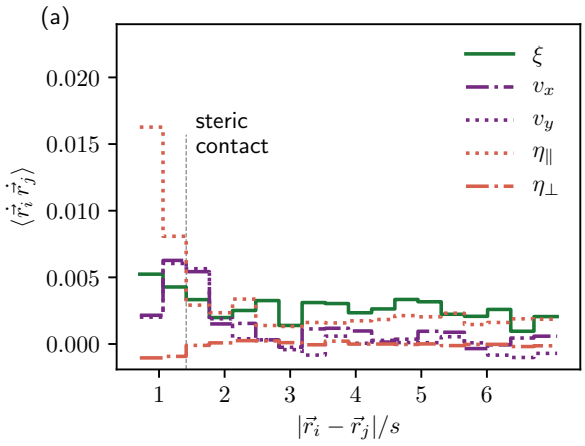

Fig. S4 Spatial inter-particle velocity–velocity correlations in the noise. Shown are rotational (ξ, in units of rad$^2 f^2$) and translational (in units of $s^2 f^2$) velocity in both the lab (v_x, v_y) and body ($\eta_\parallel$ and $\eta_\perp$) frame, plotted as a function of center–center separation between pairs of particles. Due to the square shape of the particles, corner–corner contact occurs at a separation of $r \approx \sqrt{2}s$ (vertical line) while face–face contact is at $r = s$.

tial correlations between particles. In figure S4, we calculate velocity–velocity radial correlations $\left\langle \dot{\vec{r}}_i(t)\dot{\vec{r}}_j(t)\right\rangle$ as a function of the pair separation distance r between two particles at a single point in time. The average is over time and all particle pairs i and j separated by center–center distance $r = |\vec{r}_i - \vec{r}_j|$. We calculate these correlations in the rotational and translational velocity in both the lab and body frames. In several components of the velocity, correlations due to steric interactions appear at closest contact ($r = s$) and, due to the square particle shape, persist toward the furthest reach of interactions at the corner–corner contact $r \approx \sqrt{2}s$. Beyond this range, correlations vanish in all velocity components.

References

1 J. L. Doob, *Annals of Mathematics*, 1942, **43**, 351–369.

2 T. E. Oliphant, *Computing in Science & Engineering*, 2007, **9**, 10–20.

3 S. van der Walt, S. C. Colbert and G. Varoquaux, *Computing in Science and Engineering*, 2011, **13**, 22–30.

4 L. Walsh and N. Menon, *J. Stat. Mech.*, 2016, **2016**, 083302.

5 S. van der Walt, J. L. Schönberger, J. Nunez-Iglesias, F. Boulogne, J. D. Warner, N. Yager, E. Gouillart and T. Yu, *PeerJ*, 2014, **2**, e453.

6 E. Jones, T. Oliphant, P. Peterson and others, *SciPy library: Open source scientific tools for Python*, SciPy contributors, 2001.